Fabrication of Polymer Surfaces with Varying Roughness and Its Effect on Anti-Reflective Properties

Suresh Killada

A Dissertation Submitted to

Indian Institute of Technology, Hyderabad

In Partial Fulfilment of the Requirements for

The Degree of Master of Technology

मारतीय प्रौद्योगिकी संस्थान हैदराबाद
Indian Institute of Technology Hyderabad

Department of Chemical Engineering

June, 2014

i

Declaration

I declare that this written submission represents my ideas in my own words and where others' ideas or words have been included, I have adequately cited and referenced the original sources. I also declare that I have adhered to all principles of academic honesty and integrity and have not misrepresented or fabricated or falsified any idea/data/fact/source in my submission. I understand that any violation of the above will be a cause for disciplinary action by the Institute and can also evoke penal action from the sources that have thus not been properly cited, or from whom proper permission has not been taken when needed.

(Signature)

Suresh Killada

(CH12M1005)

Approval Sheet

This thesis entitled "Role of Polymer Surface Roughness on Its Optical Properties" by Suresh Killada is approved for the degree of Master of Technology from IIT Hyderabad.
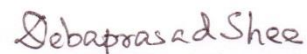
Dr Siva Rama Krishna

Department of Electrical Engineering
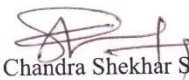Indian Institute of Technology Hyderabad
Examiner

Dr Saptarshi Majumdar

Department of Chemical Engineering
Indian Institute of Technology Hyderabad
Examiner

Debaprasad Shee
Dr Debaprasad Shee

Department of Chemical Engineering
Indian Institute of Technology Hyderabad
Examiner

Dr Chandra Shekhar Sharma

Department of Chemical Engineering
Indian Institute of Technology Hyderabad
Advisor

iii

Abstract

Any real surface is rough at some length scale. Surface roughness plays an important role in various physical properties including light scattering phenomenon. In first part of the work, we have chosen electrospun nanofibers mat first time to the best of our knowledge, as a model polymer surface of varying roughness. We have varied the surface roughness by electrospinning cellulose acetate based nanomaterials, like only beads to fibers. Spin coated thin film was considered as a reference sample. Cellulose acetate was an obvious choice for selection of polymer due to its low refractive index, 1.47. Surface morphology and roughness of prepared samples was characterized using scanning electron microscopy (SEM) and 3-D non contact optical profiler. Optical properties were characterized using by measuring specular reflectance/transmittance in the visible spectral range by using UV-VIS spectrophotometer. These results showed that cellulose acetate surfaces with only beads morphology show near zero reflection ($< 0.1\%$) for a wide range of wavelength. For only beads as well as only fibers morphology, cellulose acetate surfaces showed <0.16% reflection while varying the angle of incidence of light from 30º to 75º while transmittance was also reduced to less than 5%.

Further we have chosen PS-b-PMMA block copolymer (BCP) and fabricated rough and porous surfaces by inducing phase separation using solvent/non-solvent exchange. We have shown that by choosing different combinations of solvent/non-solvents, we can vary the surface roughness at nanoscale. These rough BCP surfaces were further tested for their optical properties and results confirmed broadband and omnidirectional near-zero reflection behavior for these surfaces as well.

Finally nano and micro scale rough surfaces as fabricated in this work due to their anti-reflective nature may find potential applications in solar panels, marines, optical displays etc.

Dedication

Dedicated to teachers and friends for their ever present support

Acknowledgments

Nomenclature

Gm	Grams
AOI	Angle of Incidence
AR	Anti-Reflective
DMA	Dimethylacetamide
DMF	Dimethylformamide
RMS	Root Mean Square
UV-VIS	Ultra Violet- Visible
Nm	Nanometer
T_g	Glass Transition Temperature
SEM	Scanning Electron Microscope
PS-b-PMMA	Polystyrene-b-poly(methyl methacrylate)
BCP	Block copolymer
THF	Tetrahydrofuran
Mw	Weight molecular average
Mn	Number molecular average
BSE	Back Scattered Electrons
I	Intensity
3D	Three dimensional
N	Refractive index
R%	percentage of reflection
T%	percentage of transmission
Ml	Milliliter
SDFCL	S D Fine-Chem Limited
Kv	Kilovolts
µl	Microliter
Cm	Centimeter
DI	De-ionized (water)
Mm	Millimeter

List of figures:

List of Tables

Table of Contents

Chapter 1: Introduction

Chapter 2: Fabrication of Polymer Surfaces with Variable Roughness

Chapter 3: Optical Properties of Rough Polymer Surfaces

Chapter 1

Introduction

1.1 Optically Active Surfaces

Nowadays, nano porous films are widely employed in numerous applications or in opt photonic devices such as displays [1], solar cells [2-4], or light-guiding [5-6] systems. In particular, the technological feasibility of nano porous layers with low refractive indices has recently enabled the development of high-efficiency anti-reflection coatings.

The formation of a porous structure in thin film gives place to a layer with the adequate refractive index for obtaining the antireflective property. To obtain potential of such films for broadband AR (Anti-Reflective) applications by combining them in a graded-index multilayer that reduces the surface reflectivity of a polymer substrate from 10% to few % is hopeful challenge. Since from 1990s, both inorganic and organic nano porous layers have appeared as very attractive materials with many potential applications in the fields of biochemistry, electronics, optics, and photonics [7].

Nanostructured composite films have also been developed for optical applications such as light harvesting and energy conversion in solar cells. Moreover, the introduction of low-n films has represented a very important break-through in the development of interference antireflection coatings, which play a pivotal role in a wide variety of optical devices by increasing light transmission at the interfaces, i.e., by eliminating unwanted reflections and glare. The basic principle of AR films is based on glass and common plastics have n values in the range1.45-1.7

and, consequently, they reflect up to 10% of normal incident light. Materials with refractive index 1.2–1.3 are required for achieving efficient AR coatings, and to overcome this issue, since the 19th century, non-porous materials have been proposed for AR applications. If the pore size is much smaller than the wavelength of light, the average n value can be drastically reduced with a very limited light scattering. AR coatings with minimum reflectivity of a 1-2 % in the visible spectral range over a wide range of incidence angles helps in lowest attainable n values are around 1.35.

Recently, a technology that has contributed significantly in improving the visibility of pavement markings and road signs named as retro reflectivity. Many highway signs and pavement markings use special sign sheet and pavement marking materials that send a large portion of the light from a car's headlights straight back along the same path from which it came. This is known as Retro reflection.

Polymer films [8] are clear enough to replace glass, their low glass transition temperatures (Tg) render them unstable at high temperatures and long anneal times. Several deposition techniques for thin film fabrication such as vacuum evaporation [9] sol–gel method [10, 11] and magnetron sputtering [12-13], chemical vapor deposition [14] have been widely used. The properties of the thin film silicon solar cells, can be improved using textured silicon wafers, but still limited by a few technological issues such as the difficulty of uniformly coating etc. Broad-band AR films were thus obtained that reduce the surface reflection from10% to few % in the visible region. Here in this study we deposited cellulose acetate nanofibers on the silicon wafer. The nanofibers were generated by using electrospinning technique.

1.2 Objective and lay out of the thesis

2

A polymer precursor material, cellulose acetate was used for preparing continuous nanofibers. Fibers were deposited on silicon wafer by using electrospinning technique. The refractive index of Cellulose acetate is 1.47

Due to its biodegradable nature, renewability, non-toxic   good thermal stability and chemical resistance of cellulose acetate, researchers trying to modify its physical properties and chemical structure for improving its properties, so that it can be used wide range of applications. The glass transition temperature of cellulose acetate is 200ºC-300ºC and melting temperature is close to 260ºC. The reactivity of cellulose acetate is more with the water.

Cellulose acetate has been extensively used for preparing of nano fibers by electrospinning process [14] .By mixing of polar and non-polar solvents, a good smooth long nano fibers can be generated. Beads will be formed in using one solvent system [15-16]. Organic solvents like acetone used for solution preparation because of less crystalline nature .some other solvents like dimethyl acetamide and other ionic liquid were also used to prepare electro spun cellulose nanofibers

Lay out of the thesis is shown below:

```
┌─────────────────────────────────────┐
│      Cellulose acetate  solution     │
└─────────────────────────────────────┘
                   ⬇

┌─────────────────────────────────────┐
│ Electrospinning of cellulose acetate polymer │
└─────────────────────────────────────┘
                   ⬇

┌─────────────────────────────────────┐
│ Optimizing parameters  to fabricate  cellulose acetate nano │
│                                      │
│                fibers                │
└─────────────────────────────────────┘
                   ⬇

┌─────────────────────────────────────┐
│           Characterization           │
└─────────────────────────────────────┘
                   ⬇
```
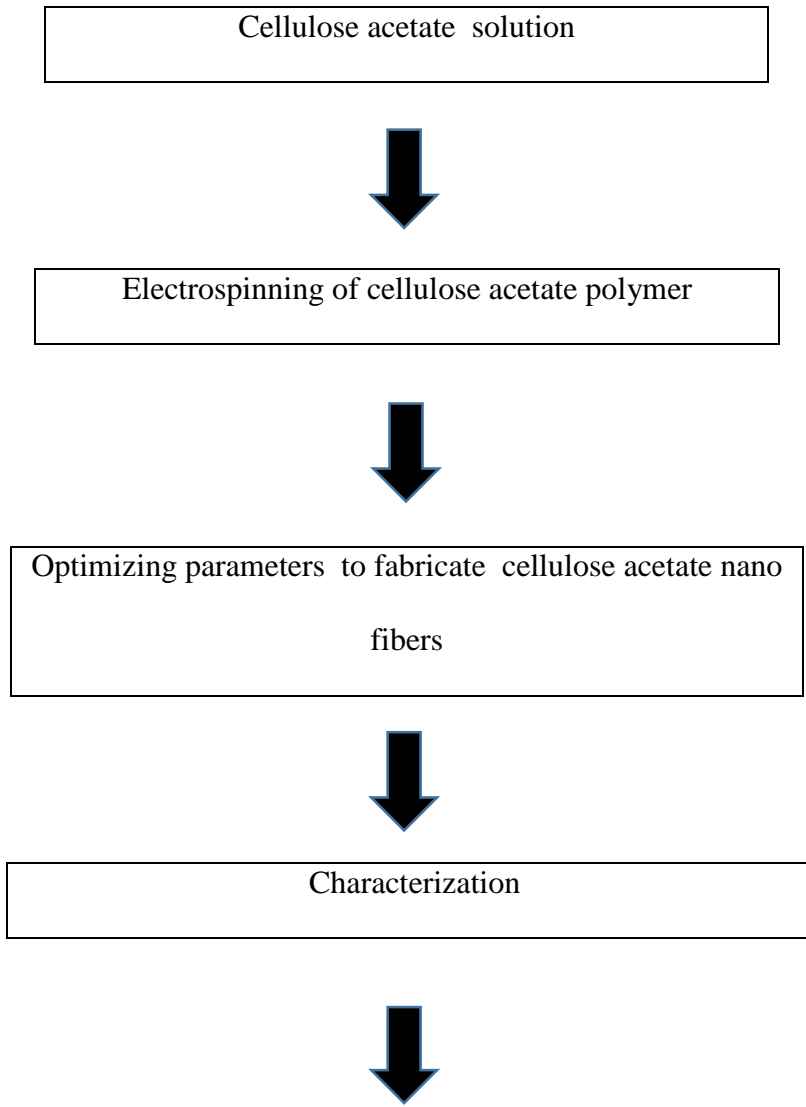
1	Surface morphology	SEM(Scanning Electron Microscopy)
2	Surface roughness	3D Optical Profiler(Non-Contact Mode)
3	Optical Properties	UV-VIS Spectrophotometer(visible region)

Chapter 2

Fabrication of polymer surfaces with variable roughness

2.1 Electrospinning:

Among the most successful methods for producing nanofibers, electrospinning process stands as a cheap and efficient method. In this process we use high electric charge to draw very fine (typically on the micro or nano scale) fibers from a wide variety of natural and synthetic polymers. A polymer solution is injected at a constant feed rate though a needle which is charged to a high voltage, typically 10 to 20 kV. The applied voltage induces a charge on the surface of the liquid droplet and when this is sufficiently high, the hemispherical surface of the fluid elongates and a Taylor cone is established. On increasing the applied voltage further charged liquid jet will eject from the Taylor cone and attracts towards the collector, which is positioned at a fixed distance from the needle. During this process the solvent evaporates from the polymer solution, leaving dry polymer fibers on the collector. Electrospinning set up mainly consists of high voltage power supply, syringe pump and a collector screen.

The variable factors of electrospinning process include applied voltage, diameter of needle used, flow rate of the solution, distance between the source and the collector, temperature and humidity during the spinning process. By optimizing all the parameters, electrospin nano fibers with desired morphology can be produced.

2.1.1 Materials

Cellulose acetate (acetyl content 39.8%, molecular weight 29000) was purchased from Sigma Aldrich, India. NN-Dimetylacetamide (DMA) (99.5% pure), was purchased from Merck specialties private limited, India whereas acetone (99%pure) was purchased from Vetec, India. These are the chemicals which were used throughout the experimental process for solution preparation without any further modification.

2.1.2 Sample Preparation

Precursor solution of cellulose acetate of concentration 16wt% & 8wt% were prepared by using acetone and Dimethylacetamide (DMA) solvents in 2:1 molar ratio. The solution is stirred at room temperature until a transparent homogenous solution was obtained. Prepared so
.We have studied the effect of various parameters i.e., voltage, the distance between the tip and the collector, needle gauge and the flow rate of the solution on the morphology of the fibers. These parameters have been optimized to yield continuous nanofibers.

Cellulose acetate nanofibers on silicon wafer were deposited by electrospinning technique. Here we used 24 gauge (ID 0.31mm) syringe needle connected to high voltage power supply. An electric potential difference, of 10 kV, is established between the surface of the polymer drop and the collector plate separated by a distance of 10 cm horizontally. The fiber deposition time was fixed for 30 minutes. Silicon wafers of 2cm×2cm size were used as substrate. The flow rate of 1kV/cm was initialized
A number of experiments were conducted to get these favorable parameters to generate the uniform continuous cellulose acetate nanofibers with thin diameter.

2.1.3 Cellulose acetate thin film preparation

Usually a small amount of polymer material is applied on the center of the substrate and then substrate rotated at high speed in order to spread the coating polymer by centrifugal force acting outwards the center.in spin coating. Spin coating is widely used in the semiconductor industry, where it can be used to create thin films with thicknesses below 10 nm. It is also used intensively in photolithography, to deposit layers of photoresist about 1 micrometer thick. Here we used Silicon wafers of 2cm×2cm size as substrate. The parameters, morphology, methods, and conditions are shown in the table below. Here along with the nanofiber samples, we have spin coated cellulose acetate polymer on clean Si wafer at 3000 rpm to get uniform thin films. Table 1 shows the methods and conditions for fabrication of different morphological structures.

Table 1: Summary of the methods and experimental parameters for cellulose acetate based electrospun nanostructured surfaces

MORPHOLOGY	METHOD USED	CONDITION USED
THIN FILM	SPIN COATING	3000 RPM, For 20 SEC Polymer Conc.: 8 wt.% and 16wt.%
BEADS	E-SPRAYING	Polymer Conc. : 16 wt.% Flow rate : 1μL/min Distance between tip of the syringe and collector: 10cm Voltage applied: 1KV Deposition time: 30min Substrate used :Silicon wafer
PLAIN FIBERS	E-SPINNING	Polymer Conc. : 8 wt.% Flow rate : 1μL/min Distance between tip of the syringe and collector: 10cm Voltage applied: 1KV Deposition time: 30min Substrate used :Silicon wafer

2.1.4 Surface morphology analysis

The obtained fibers from the two set of experiments were characterized by SEM (Scanning Electron Microscope) imaging. SEM produces images of a sample by scanning it with a focused

8

beam of electrons. The electrons interact with the atoms of the sample which produces signals that can be detected and provides the information about the surface's topology and composition. The signals that derive from electron reveal information about the sample including external morphology (texture), chemical composition, and crystalline structure making up the sample. In most applications, data are collected over a selected area of the surface of the sample, and a 2-dimensional image is generated. Areas ranging from approximately 1 cm^2 to 5 microns in width can be imaged in a scanning mode using conventional SEM techniques (magnification ranging from 20X to approximately 100,000X, spatial resolution of 50 to 100 nm). Accelerated electrons in an SEM carry significant amounts of kinetic energy, and this energy is dissipated as a variety of signals produced by electron-sample interactions when the incident electrons are decelerated in the solid sample. These signals include secondary electrons (that produce SEM images), backscattered electrons.

Fiber morphology was studied using Desktop SEM (Phenom) as shown in figure 1.. As after the SEM analysis the fibers at 16 wt% obtained were found to be uniform continuous fibers .Similarly when 8wt% samples are found to be only beads.
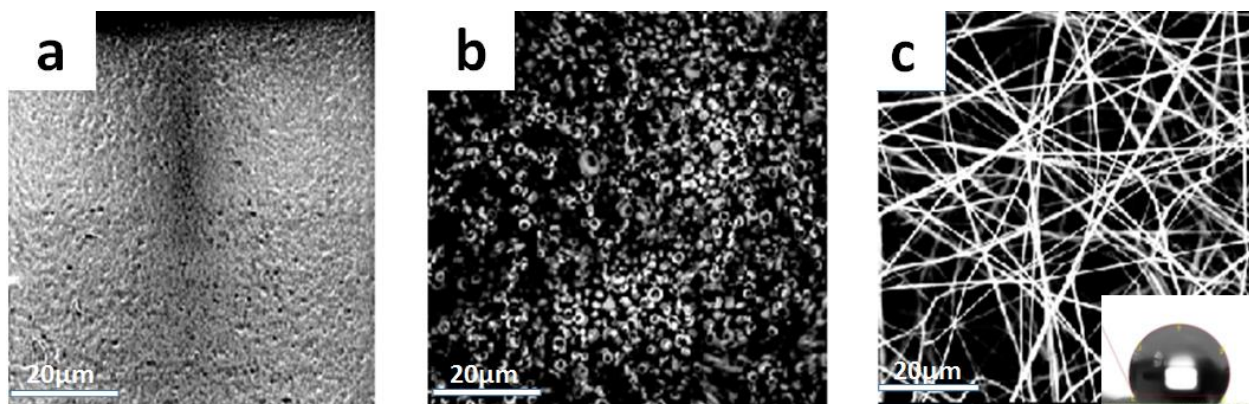
Fig **1**.SEM images of different morphologies (a) Spin coated 40 micron thickness film (b) Doughnut shaped beads (c) Continuous nanofibers (c) shows contact angle 117º(hydrophobic)

Here we found clear distinguished nanofibers generated for 16wt% molar concentration. The average fiber diameter is around 170nm. Figure 8wt% molar concentration, we found formation of beads. The interesting thing found is, beads are doughnut shaped. Further research is yet to be done to understand the doughnut bead formation. In both the cases we maintained 1µl/min flow rate.

2.1.5 Surface Roughness Analysis

Surface roughness, often shortened to roughness, is a measure of the texture of a surface. It is quantified by the vertical deviations of a real surface from its ideal form. If these deviations are large, the surface is rough and if they are small the surface is smooth. Increase in the surface roughness of samples results in increase of surface area, thus helps in enhance of anti-reflective properties. The light trapping in between the surface projections at nano level, thus opens a new front in developing efficient handling as light harvesters. The surface roughness of the samples were analyzed by optical profiler in non-contact mode. The leading method of this type is light. Light emitted from the instrument is reflected and read, to measure without touching the sample. Various non-contact systems include the focus detection type, the confocal microscope type, and the interferometer type. As they are non-contact, these systems never harm the sample and can even measure soft or viscous materials. The Root Mean Square (RMS) value was determined by taking the mean of the RMS measurements at the three different places on the same sample surface. The non-contact profilometer does not touch the surface the scan speeds are dictated by the light reflected from the surface. A typical profilometer can measure small vertical features ranging in height from 10 nanometers to 1 millimeter. Projecting a narrow band of light onto a three-

dimensionally shaped surface produces a line of illumination that appears distorted from other perspectives than that of the projector, and can be used for an exact geometric reconstruction of the surface shape. The root mean square also known as the quadratic mean, is a statistical measure of the magnitude of a varying quantity. We used Nanomap (AEP technologies) 3D profiler for measuring roughness of nanofibers, porous films and thin films as spin coated.

Optical Profiler 2D images
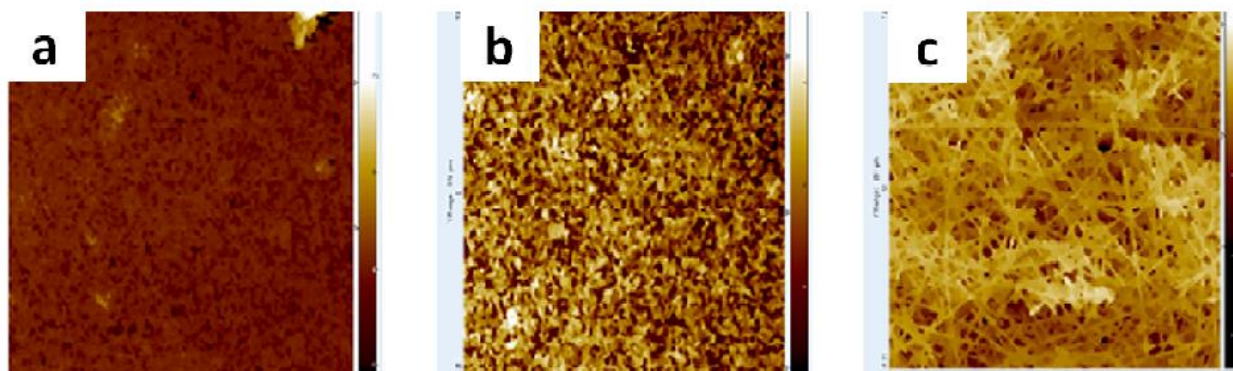
Fig 2.Optical profiler 2d images of different morphologies (a) Spin coated 40 micron thickness film (b) Doughnut shaped beads (c) Continuous nanofibers

The stage on the optical profiler was moved and an image was taken at four different places .The profiler images readily allowed in the identification of different roughness morphological structures. Varieties of scans were acquired at random locations on the film surface. As the light of high intense is focused on the sample surface, the reflections from a smooth surface are reflected back at the angle of incidence, and the material appears glossy. If the surfaces are rough, the surface structure scatters the incident light resulting in wide and narrow angle scattering. Wide angle

scattering reduces contrast and results in a milky or cloudy appearance and the magnification of the profiler image is changed by adjusting the length of the scan on the substrate .We tried at different magnifications. The current resolution images are taken at 20 x .Here from the obtained optical profiler 2d images we clearly differentiate the change in the surface morphology compared with the standard film (a) .The variation of surface roughness of samples is easily observed.

3D surface roughness analysis

The surface roughness was measured using root mean squared roughness (RMS), which is the root mean square average of the profile height deviations taken within the evaluation length and measured from the average height. RMS is the deviations of the peaks and valleys and is the preferred quantity for roughness for optical properties in coating technologies. The RMS value is much more sensitive to the magnitude of the peaks and valleys than the other methods. A detailed observation with respect to the RMS values of each sample is summarized below.
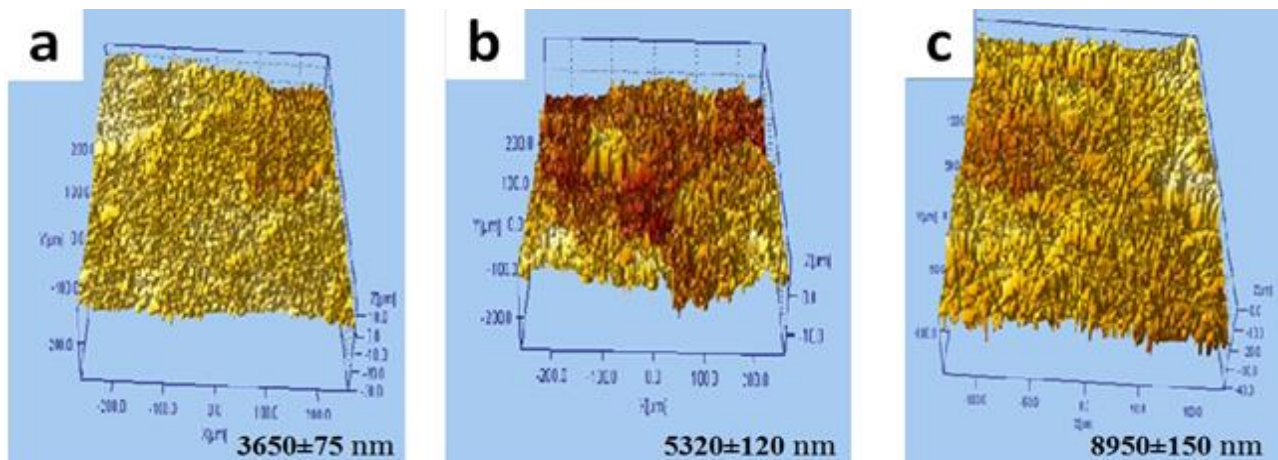

Fig **3.** 3-D Images of sample surfaces measured with profiler in non-contact mode. (a) Thin film; (b) only beads; and (c) only fibers. Values reported are root mean square surface roughness

The deposition period is same for all the samples. The thickness of the deposited samples is ~ 40μm. As can be see, three typical morphological features are recognized readily by visual inspection of Figure 3. Figure 3a shows the smooth plain with least roughness with small features evenly places throughout the sample. In second case (Figure 3b), the granules possess different irregular shapes, sizes, and separations as beads which enhances the roughness. In the third case Fig. 3c the fibers with high surface area as well as height to width ratio enables to get higher rms value of roughness as compared to plain films and beads. The average RMS roughness and the thickness of the plain fiber samples were determined to be 8950.525±150 nm and 40±2 μm. Similarly for the beads the value is 5320.09±120 nm. By using optical profiler the step thickness of the deposited fiber sample was determined. We prepared standard films of similar thickness using spin coater and found there is drastic variation of RMS value compared to beads and fibers. The RMS value of standard film for two different concentrations (8wt% beads and 16wt% fibers) is 3650±134 nm and 3720±210 nm. Though the deposition time is same for both samples the fibers shows more roughness compared to beads. The roughness average (Sa) and the rms value were more than doubled, comparing with smooth films. A surface with a too high RMS roughness (typically more than 150 nm) is desirable since it may cause the incident light, particularly of short wavelengths to be scattered at a very high angle get absorbed due to multiple internal reflections. The high roughness RMS suggests effective scattering of the incident light at the front surface of the substrate which would help in increasing optical path length of the light inside the substrate surface and may help in achieving the minimum reflection.

2.2 Non- solvent induced phase separation

This phase separation is also referred to as "Liquid-Liquid phase separation". Phase separation can be observed by simply changing pH, temperature or reagent conditions and concentrations of the solvents used. There are several ways to prepare porous polymeric films, such as sintering, stretching, track etching and phase separation processes. The final morphology of the films and membranes obtained will vary greatly, depending on the properties of the materials and the process conditions

The concentration of the various components will be different in each of the two phases. In phase separation droplets/pores formed may be few big or few large, depending upon solution conditions and phase separation time. Different liquids have different properties and so, when combined, some will form a single, homogeneous mixture, miscible and solutions which do not get mixed i.e., heterogeneous gets phase separated. During phase separation, macro voids are formed that are useful in drug delivery systems, ultrafiltration, composite membrane supports, bioreactors, screen printing media and breathable fabrics [19]. Macro voids are the pores of having size 10-50μm. Phase inversion can be achieved by wet casting process, dry casting process, vapor induced phase separation, and thermally induced phase separation [20,21]. In wet cast process, polymer casting solution is immersed in the non-solvent bath which results formation of porous membranes due the solvent loss and counter diffusion of non-solvent into the availed solvent solution [22, 23]. If the drying rate of polymer coat on the surface of the substrate is high, and coating thickness is small, top surface becomes dense in polymer. This is due to high rate of solvent and non-solvent evaporation that is called trapping skinning. Once the skin formation takes place, the non-solvent penetrates the skin at the weak spots it initiates the macro voids [22, 23]. Liquid –liquid phase separation takes place when a homogeneous solution becomes thermo-dynamically unstable due to introduction of a non-solvent.

Polymeric porous films have been developed for a variety of industrial applications [24]. Examples of industrial applications are microfiltration, ultrafiltration, reverse osmosis and gas separation. Each application needs specific requirements on the material and film structure. For microfiltration and ultrafiltration, the porosity and the pore sizes of the films determine the efficiency of filtration.

2.2.1 Preparation of porous films using non-solvent induced phase separation

Phase separation of polymer solutions can be done in several ways. Before discussing these phase separation processes in detail, a short survey of the four main techniques for the preparation of polymeric films by controlled phase separation is presented [25-26].

• **Thermally induced phase separation (TIPS)**. This method is based on the phenomenon that the solvent quality usually decreases when the temperature is decreased. After the mixing is induced, the solvent is removed by extraction, evaporation or freeze drying.

• **Air-casting of a polymer solution.** In this process, the polymer is dissolved in a mixture of a volatile solvent and a less volatile non-solvent. During the evaporation of the solvent, the solubility of the polymer decreases, and then phase separation can take place.

• **Precipitation from the vapor phase**. During this process, phase separation of the polymer solution is induced by penetration of non-solvent vapor in the solution.

• **Immersion precipitation.** A polymer solution is cast as a thin film is immersed in non-solvent bath. Precipitation can occur because the good solvent in the polymer solution is exchanged for non-solvent.

Here we tried to study the role of surface roughness of PS-b-PMMA polymer films on its optical properties. We choose non-solvent induced phase separation technique to fabricate these porous films. This technique is a simple, efficient, and cheap method to prepare block-copolymer porous films by using unique phase-separation structures on the surface of polymer thin films.

Tetrahydrofuran (THF) and dimethylformamide (DMF) were used as solvents to prepare aqueous suspensions of nanoparticles of the block copolymers.

2.2.2 Materials

PS-b-PMMA block copolymer with molecular weight (Mw) 52000-25000 g mol^{-1} were purchased from Fischer Scientific, India. DMF (99% purity) was purchased from SDFCL Limited. THF (99%purity), and ethanol (99% purity) were purchased from Merck India. All the chemicals were used without any modifications.

2.2.3 Solution Preparation

2 wt% PS-b-PMMA solutions were prepared by dissolving it in DMF and THF solvents at room temperature using a magnetic stirrer until a transparent homogenous solution was obtained. Silicon wafers of 2cm×2cm size were used as substrate.

2.2.4 PS-b-PMMA block copolymer films by spin coating

Using dropper, PS-b-PMMA solution (DMF as solvent) is taken and spin coated at 2000 rpm for 20 sec. Once the film was fabricated with no time gap, a few drops of ethanol (non-solvent)was spin coated at 1000 rpm for 10 sec .Similarly with no change in parameters one more sample was prepared using DI water (non- solvent.

Now the same process is continued for PS-b-PMMA solution (THF as solvent), two more samples were prepared using same non-solvents using the same parameters.

In order to compare the results, a set of standard samples i.e. PS-b-PMMA block copolymer films with both THF and DMF solvents only separately were prepared. A total six number of samples were prepared.

2.2.5 Surface morphology analysis

After preparation of six samples on silicon wafers of 2×2cm size, the surface morphology analysis were done by using SEM (Phenom World).
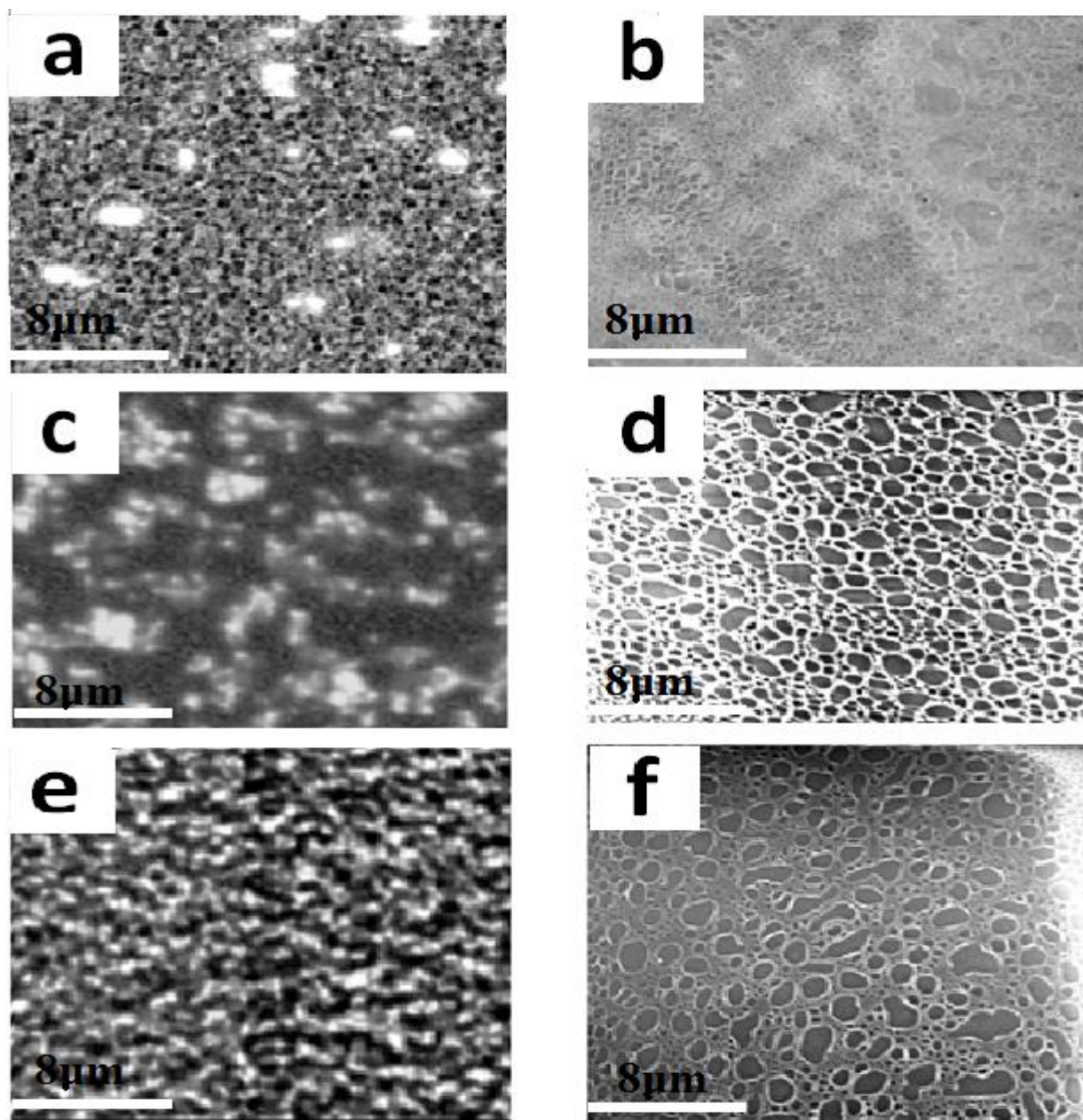
Fig **4**: SEM images of PS-b-PMMA polymer porous films.(a) DMF solvent standard porous film (b) THF solvent standard porous film (c) DMF solvent and DI water as non-solvent) porous film (d) THF solvent and DI water as non-solvent (e) DMF solvent and ethanol as non-solvent (f) THF solvent and ethanol as nonsolvent.

All SEM images are taken at 10000x magnification. Here we observe both the porous films (d) PS-b-PMMA (THF solvent) and DI water as non- solvent and (f) .PS-b-PMMA (THF solvent) and ethanol as non–solvent are showing high porosity. If a solution of a polymer in a solvent of lower molecular mass exhibits liquid-liquid demixing, then a strongly asymmetric liquid-liquid demixing gap is observed. The phenomenon of separation into coexisting liquid phases signifies attractive interactions between the molecules. Such attractive interactions can also lead to crystallization and aggregation of the molecules. The process of separation occurs very slowly due to viscosity of solution and entanglement of chains (chemical cross linking reaction). Depending on the polymer concentration of the solution, liquid-liquid demixing proceeds according to different mechanisms. When the porous films were prepared using DI water as non-solvent, the porosity observed was low compared with ethanol as non-solvent. This can be clearly observed from the figure (c) & (e) figures when compared with figure (d) & (f). The standard films also showed small porous structures on the surface. Overall, the phase separation technique clearly shows increase in porous structures, and thus increased surface roughness of the films. Here the experimental data suggests the phase separation occurs in two stages leading to the so called dual morphology. Because of spinoidal mechanism (the kinetic process of spontaneous formation and continuous growth of one phase in the instable another phase) and the low viscosity of the system macro scale phase separation of domains of various compositions will occur. As the reaction proceeds there occurs abrupt change in the equilibrium composition of phases in a short period of time. This results in dual phase morphology

2.2.6 Optical microscope images

Here we observe a clear dual phase morphological structures on surface of the porous films. All the images were taken at 20x magnification, showing a clear distinctive phase separation. It shows that heterogeneous structures arise due to micro phase separation.
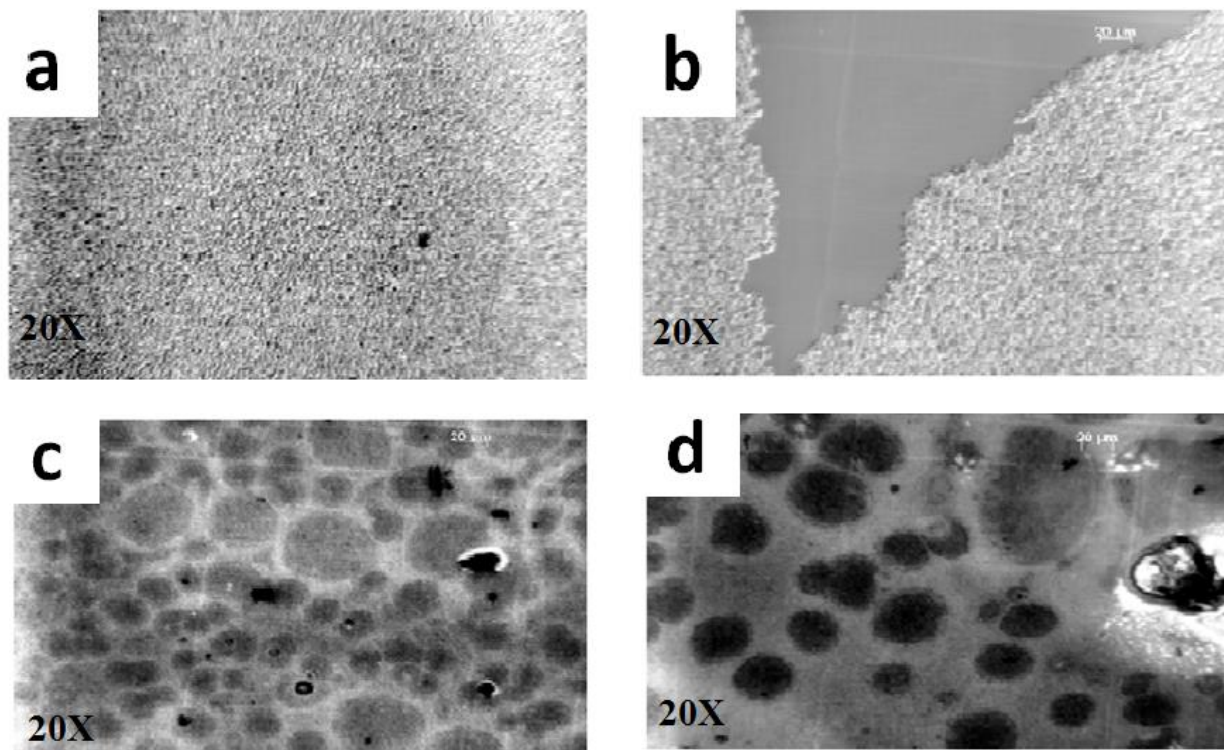

Fig **5**: Optical Microscope images of PS-b-PMMA porous films at 20x magnification (a) DMF solvent and ethanol as non –solvent (b) DMF solvent and DI water as Non-solvent (c)THF solvent and DI water as non –solvent) (d) THF solvent and ethanol as non -solvent

2.2.7 Surface roughness analysis

Surface roughness is an important parameter to be considered since it plays a significant role in Influencing the surface properties and hence the performance of materials. The effect of surface roughness on the nanoscale has been found to be important in sensing devices

The surface roughness was measured using root mean squared roughness (RMS), which is the root mean square average of the profile height deviations taken within the evaluation length and measured from the average height.

For each sample at random positions, the stage on the optical profiler was moved and surface roughness was measured at four different places in order to get the average RMS value .The profiler images readily allowed in the identification of different roughness morphological structures. The total area scan of each sample was X range = 523 µm, Y range = 523 µm and Z range varied for sample to sample. 3D profiler was operated in non-contact mode.

Here from the obtained results we found PS-b-PMMA porous films (THF solvent) and Ethanol as non- solvent showed high RMS value i.e., 3218.45±371 nm. The standard porous film shows 1186±257nm. From this we can clearly observe the role of phase separation technique in increasing the surface roughness of films. A steady increase of RMS value about 2032.45 nm shows its importance.

For PS-b-PMMA porous film (THF solvent) and DI water as non- solvent shows surface roughness equals to 2383±237 nm while it was measured to be 692±141nm for the standard porous film prepared in DMF solvent only.

A detailed observation with respect to the RMS values of each sample is summarized below
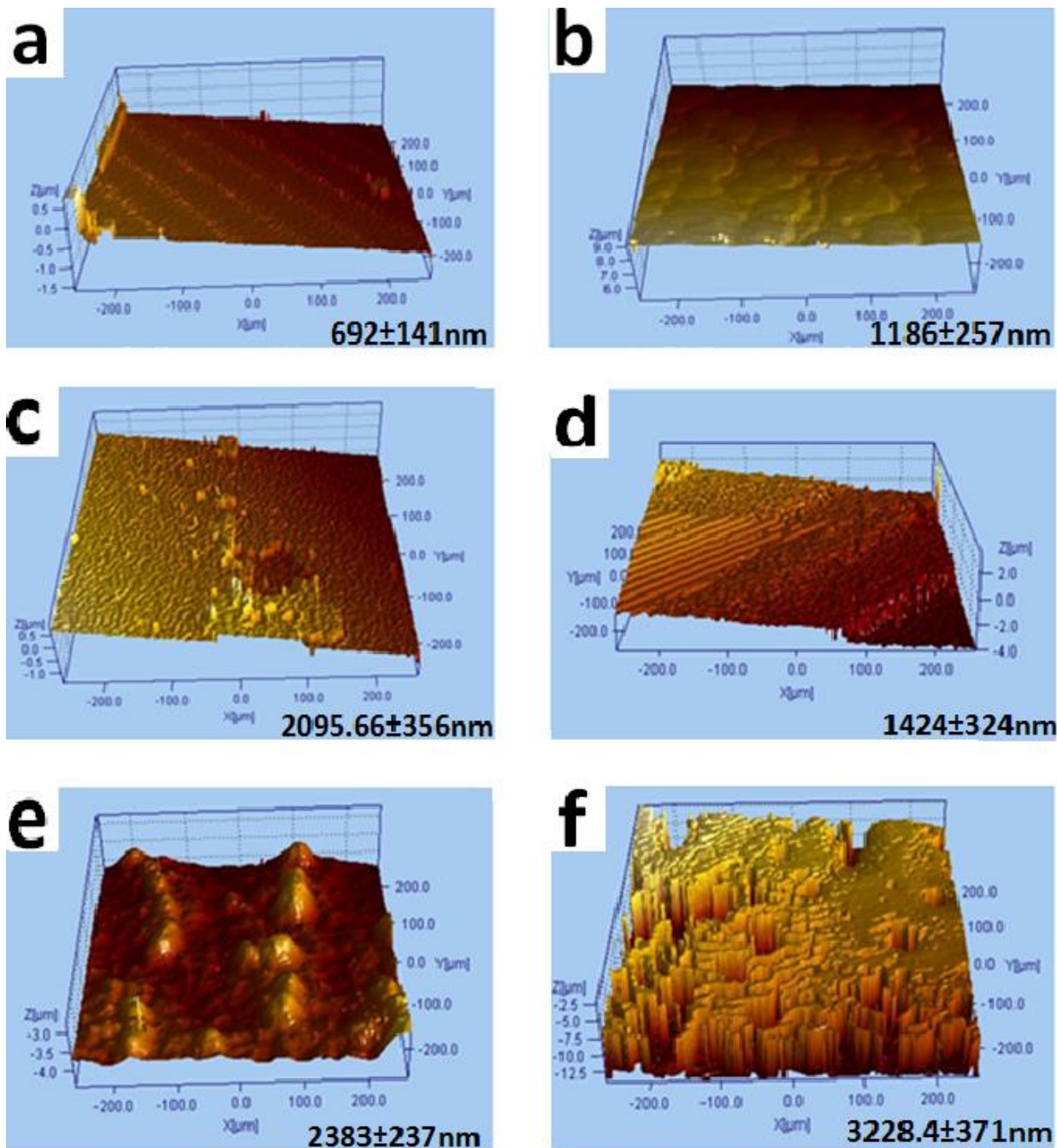
Fig **6**: 3D optical profiler images of PS-b-PMMA (a) standard porous film (DMF solvent); (b) standard porous film (THF solvent); (c) DMF solvent and ethanol as non –solvent; (d) DMF solvent and DI water as non-solvent; (e) THF solvent and DI water as non-solvent; (f) THF solvent and ethanol as non-solvent. Values reported are root mean square surface roughness.

2.2.8 AFM analysis:

The six porous PS-b-PMMA porous films were analyzed by Atomic Force Microscope (AFM). It consists of a cantilever with a sharp tip (probe) at its end that is used to scan the substrate surface. When the tip is brought into proximity of a sample surface, forces between the tip and the sample lead to a deflection of the cantilever.

Fig **7**: AFM 2D images of PS-b-PMMA (a) standard porous film (DMF solvent), (b)DMF solvent and ethanol as non -solvent (c) DMF solvent and DI water as non –solvent(d) standard porous film(THF solvent),(e) THF solvent and DI water as non- solvent .(f) THF solvent and ethanol as non- solvent .

Samples shows that thf- solvent based ps-b-pmma porous films shows a clear porous structures compared with the dmf porous films. All samples were scanned at room temperature. The porosity of (d),(e) &(f) clearly signifies the phase separation between the solvent(thf) and non-solvents (di-water and ethanol) gave better results in increasing the surface roughness of porous films.
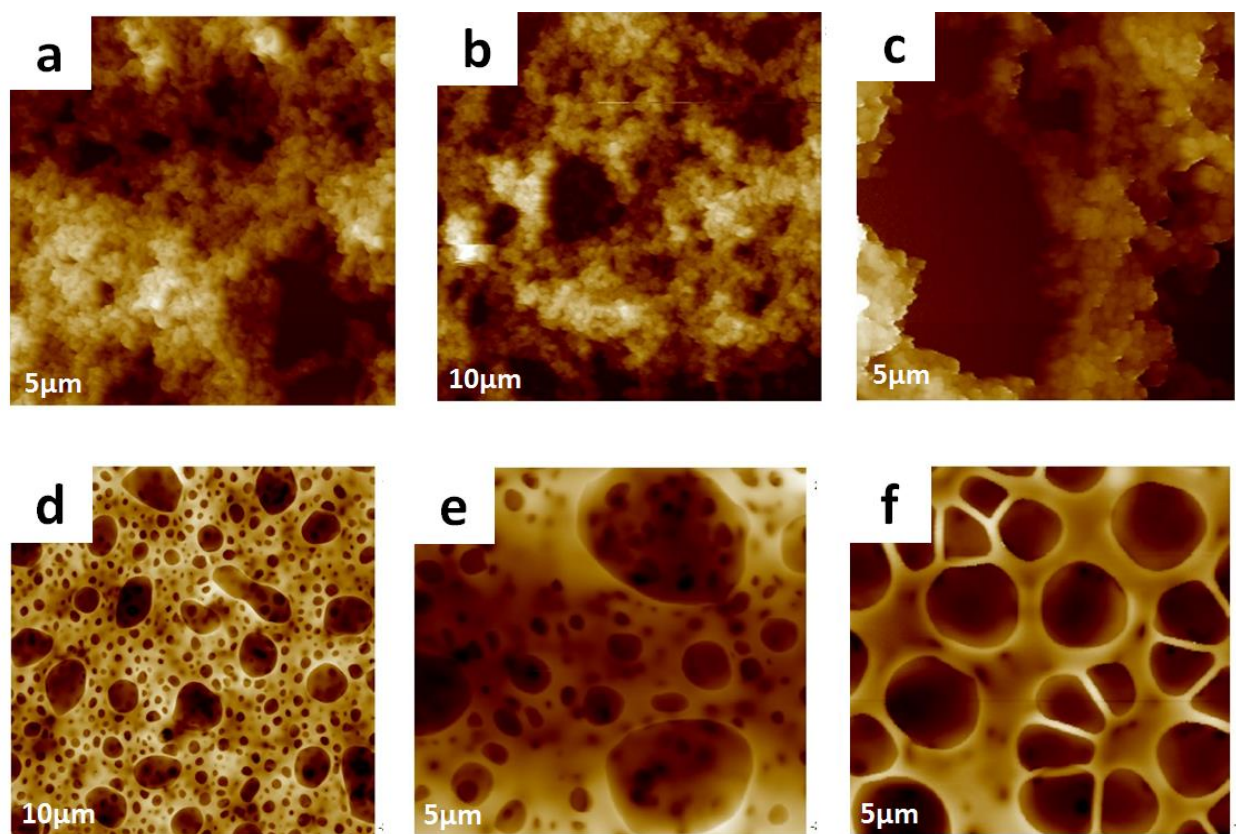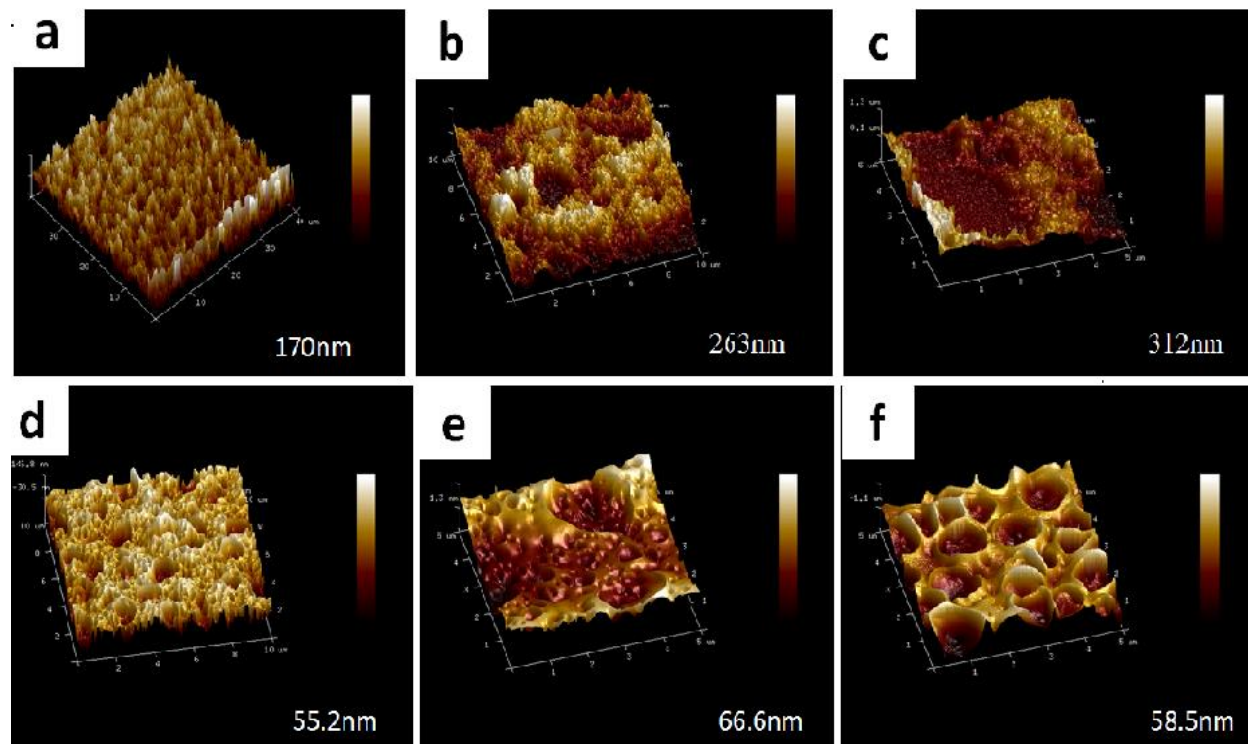

Fig **8**: AFM 3D images of PS-b-PMMA (a) standard porous film (DMF solvent), (b)DMF solvent and ethanol as non -solvent (c) DMF solvent and DI water as non –solvent(d) standard porous film(THF solvent),(e) THF solvent and DI water as non- solvent .(f) THF solvent and ethanol as non- solvent. Values reported are root mean square surface roughness.

Surface roughness of porous films was increased compared with standard porous films. Before etching images (a) and (d) shows rms values 170 nm and 55.2 nm respectively. Porous films with DMF solvent showed show high roughness values compared to THF as solvent. The etching period

was 10 sec for all the samples. When di water used for both the solvent based samples, high roughness values(c) and (e) were recorded. In DMF solvent based porous films the roughness values were doubled (c) 312nm compared with standard samples. The porous films with ethanol as non-solvent shows low rms value (b) 263nm and (f) 58.5nm compared with di water as non-solvent. The combination of DMF –DI water and THF-DI water due to change in pH, reagent conditions and concentrations of the solvents gave better phase separated porous structures. Each sample was scanned at 5, 10 and 40μm respectively. Surface roughness increased with increase in porosity. Image (e) and (c) show highly porous structures on the surface. The roughness values thus obtained suggests high light scattering during optical property analysis. The rms values suggest DI water as no solvent can be used for better phase separation compared with ethanol. All the three THF solvent based films showed low rms values (d) 52.2nm, (f) 58.66nm and (e) 66.66nm, respectively. This is due to the fact the interaction between both the phases is low and inert.

Chapter 3

Optical Properties of Rough Polymer Surfaces

3.1 Optical Properties

Optical properties are fundamental physical properties that describe the interaction between electromagnetic waves and matter from deep ultraviolet to far-infrared spectral regions. In fact, optical property measurements and analysis offer powerful tools to understand the physics of the Materials. Optical property of a material is defined as its interaction with electro-magnetic radiation in the visible. Interaction of photons with the electronic or crystal structure of a material leads to a number of phenomena. The photons may give their energy to the material (absorption); photons give their energy, but photons of identical energy are immediately emitted by the material (reflection); photons may not interact with the material structure (transmission); or during transmission photons are changes in velocity (refraction). At any instance of light interaction with a material, the total intensity of the incident light striking a surface is equal to sum of the absorbed, reflected, and transmitted intensities. Where the intensity 'I 'is defined as the number of photons countering on a surface per unit area per unit time.

Refraction

When light photons are transmitted through a material, they causes polarization of the electrons and in-turn the speed of light is reduced and the beam of light changes direction. Refraction is the bending of the path of a light wave as it passes across the boundary separating two media.

When a beam of white light passes from air into a material having an index of refraction that varies with frequency, a phenomenon known as dispersion occurs, in which different colored components

of the white light are refracted at different angles, i.e., they bend by different amounts at the interface, so that they become separated. The different colors correspond to different frequencies. Refraction is caused by the change in speed experienced by a wave when it changes medium. The more that light refracts, the bigger the difference between these two angles.

3.1.1 Fresnel Equation

Like with reflection, refraction also involves the angles that the incident ray and the refracted ray make with the normal to the surface at the point of refraction. Not only reflection, refraction also depends on the media through which the light rays are travelling.

Fresnel equation is a dimensionless number that describes how light, or any other radiation, propagates through that medium

Normally reflective surfaces display a high refractive index to the surrounding medium (air), and as such will be highly reflective

This can be demonstrated by the use of the Fresnel equations which at normal angle of incidence (AOI) will give a reflectance between two mediums of refractive indices n1 and n2

$$r = \left\{ \frac{n1-n2}{n1+n2} \right\}^2$$

3.1.2 Reflectance Studies

Reflection is the change in direction of a wave front at an interface between two different medium so that the wave front returns into the medium from which it originated.

The law of reflection says that the angle at which the wave is incident on the surface equals the angle at which it is reflected. When light strikes the surface of a (non-metallic) material it bounces off in all directions due to multiple reflections by the microscopic irregularities inside the material and by its surface.

Reflection of light may occur whenever light travels from a medium of a given refractive index into a medium with a different refractive index. In the most general case, a certain fraction of the light is reflected from the interface, and the remainder is refracted. Reflection studies were analyzed for standard film, beads, and fiber samples by using Perkin Elmer Lambda-35 UV-VIS spectroscopy. Table 2 shows the instrument settings as follows:

Start of scan range	700	nm
End of Scan range	300	nm
Scan Speed	480	nm/min
Data Interval	1	nm
Cycle count	1	
Cycle time	1	sec
Ordinate type	%R	
Slit width	2	nm
UV Lamp on	Yes	
Visible lamp on	Yes	
Lamp change over wavelength	326	nm

The solar radiation at the earth's surface is roughly located between300 nm and 3000 nm, where the Visible (VIS) radiation (light) lays between 380nm and 780 nm.

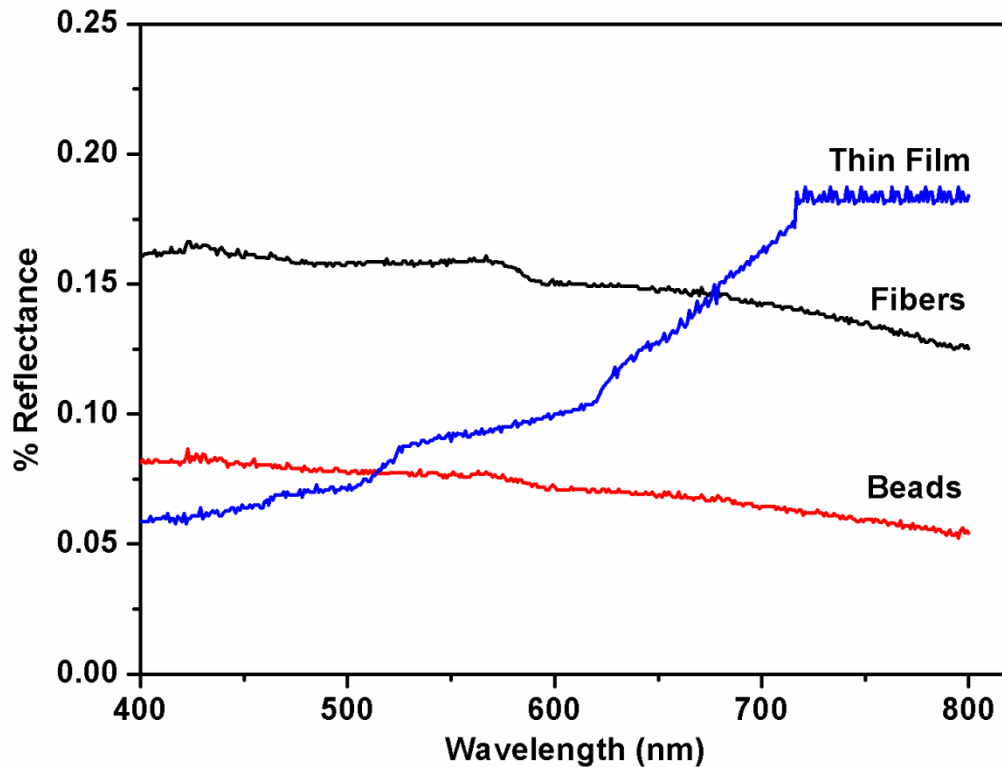### 3.1.2.1 Reflectance with variation of wavelength

Figure 9: Wavelength vs % Reflectance for fibers, beaded fibers and standard film from 400 nm to 800 nm with angle of incidence = 30deg

Here we studied the effect of surface morphology on reflectance and transmittance on variation of wavelength. We observed both the samples beads and fibers exhibit high anti- reflectivity over the entire visible range. We compared the results with standard films fabricated for both the concentrations. Here the beads showing low reflection (0.07%) compared to fibers (0.16%) constantly over the visible region. Though the surface roughness is high in fibers, due to multiple internal reflections on the surface of beads they show high anti- reflectivity.

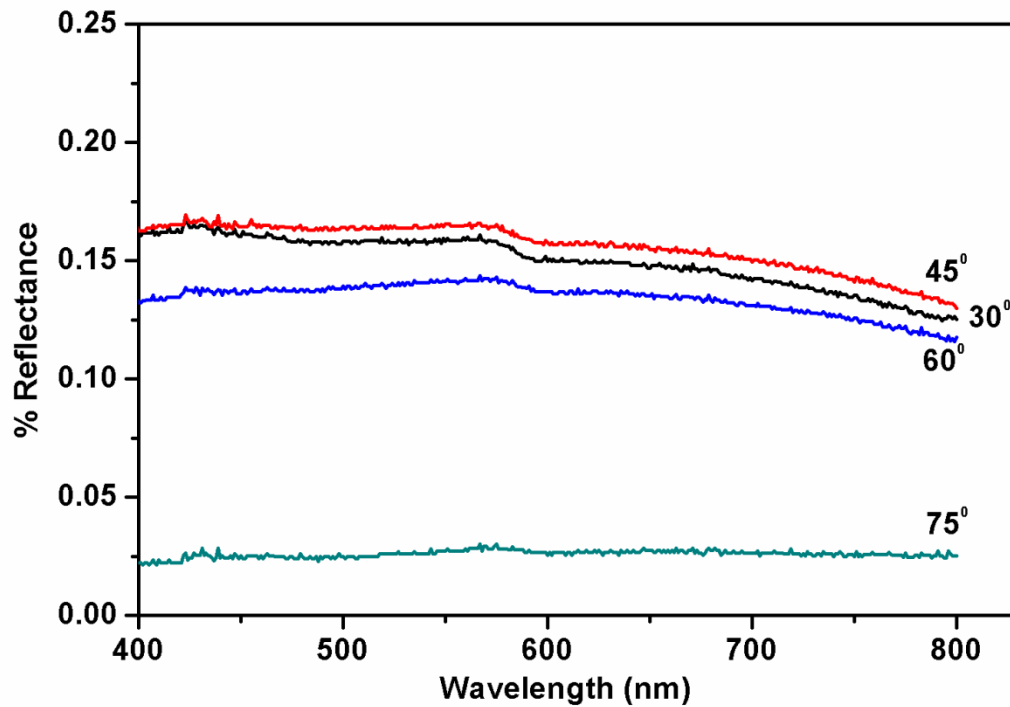### 3.1.2.2 Reflectance with variable angle of incidence

Fig **10**: UV-Vis spectra of samples at different angle of incidence. Graph shows the effect of incidence angle (30º, 45º, 60º& 75º) of light on reflectance properties for cellulose acetate fibers

Here we observe at 75º angle of incidence, reflectance is minimum (0.025%) maintaining the constant value throughout the visible region and at 45º angle of incidence a reflectance value of 0.16% was observed and gradually decreasing to 0.15% as wavelength increases.

The reflectance measurements were conducted at three different set of same samples for obtaining and maintaining the accurate values.

From the above results, the variation in angle of incidence doesn't played a major effect in altering the values and at 30º, 45º, 60º we found almost the values are merging throughout the region. At 75º incidence we observe a good variation showing high anti-reflective property compared with other values.
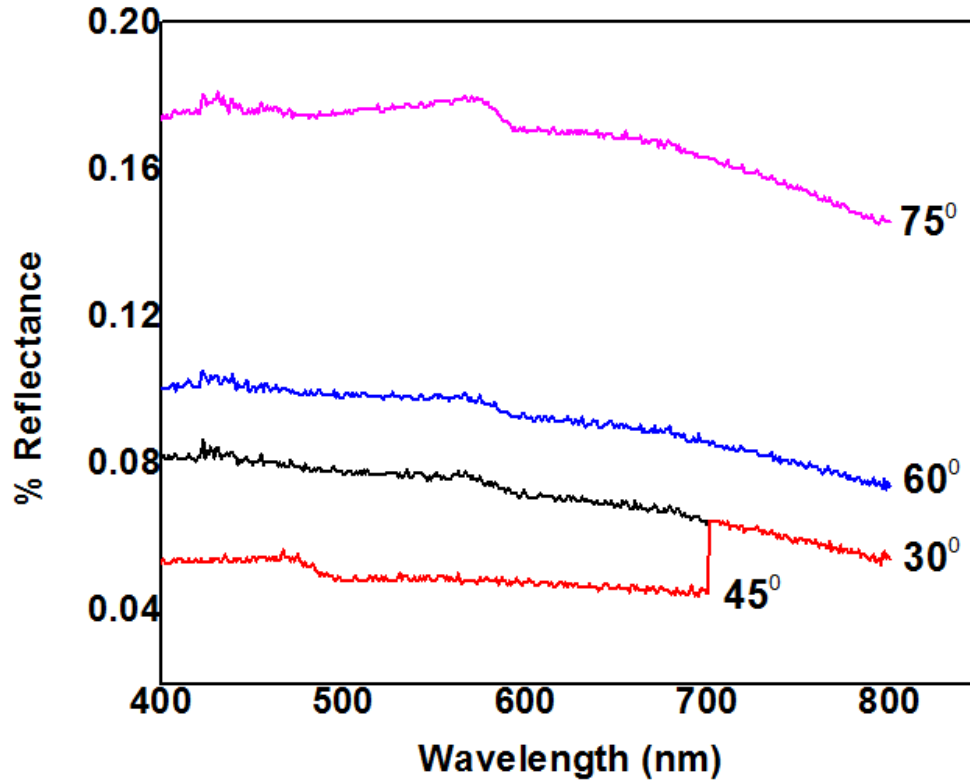
Fig **11**: Graph shows the effect of incidence angle (30°, 45°, 60°& 75°) of light on reflectance properties for cellulose acetate beads

We further studied the effect of different incidence angle of light on reflectance properties for beads a. At maximum angle, 75° beads also similar to fibers exhibit high reflectance (0.17%). As incident angle increased from 30° to 60° the reflectance value increases from 0.08% to 0.10% decreasing value as wavelength increases and converging at 0.06%.

We can conclude from these measurements that fibers as well as beads show very low reflectance values as compared to thin films. As compared with fibers, beads show much low reflectance value which is about 0.07% as of fibers (0.16%).

3.1.3 Transmittance studies

31

Fraction of light beam that is not reflected or absorbed is transmitted through the material. It is the amount of light in the visible portion of the spectrum that passes through a material.

When a light beam in impinged on a material surface, portion of the incident beam that is not reflected by the material is either absorbed or transmitted through the material. The fraction of beam that is transmitted is related to the thickness of the materials and the manner in which the photons interact with the material's structure.

Here similar to the reflectance we conducted transmittance studies and the instrument settings were not changed except the ordinate mode shifted to %T (transmittance).

As summarized in Fig. 12, it was found that an increase of average roughness promotes a decrease in transmittance. This is due to the fact that increases in deposition of beads and fibers causes a light scattering. The increase of absorbance due to increase in deposition of beads and fibers is negligible comparison to scattering effect. Here the Beads (5%) and fibers (1%) low transmittance exhibiting almost constant values over entire UV-visible region.
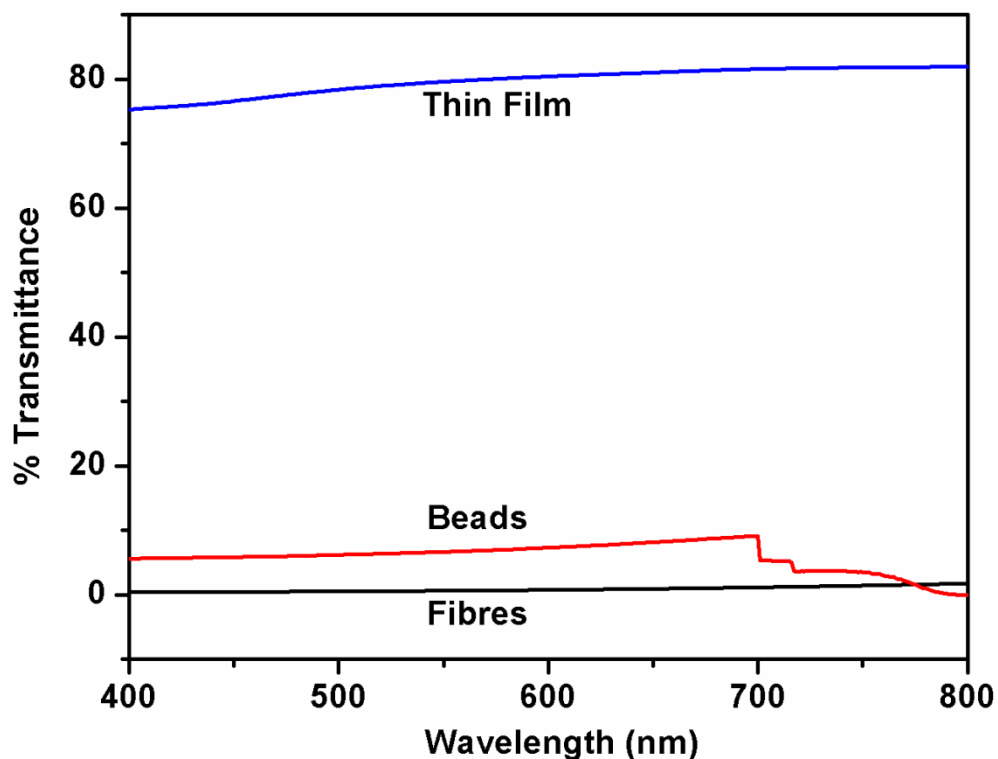
Fig 12: UV-Vis spectra showing the effect of surface morphology on transmittance with variation of wavelength.

Both the total and the specular reflectance/transmittance were measured in the visible spectral range by using UV-VIS spectrophotometer. The low reflectance (0.16%) & low transmittance (1%) measurements shows high absorbance of cellulose acetate fibers shows a good sign of using the polymer as antireflective coating applications. In this work, we propose a low cost material to be used as an excellent absorber for solar collectors, to increase its thermal efficiency by the high capacity to absorb solar radiation.

3.2 Optical property analysis for porous films as prepared by non-solvent induced phase separation

Reflection studies were analyzed for all the six PS-b-PMMA block copolymer porous films and by using Perkin Elmer Lambda-35 UV-VIS spectroscopy. The instrument settings were as follows. The instrument settings which were used for earlier studies were maintained the same.

3.2.1 Reflectance studies

Visible light represents a range of electromagnetic spectrum of wavelengths from about 350-750 nm range that can be seen by human eye.Here we studied the effect of porous structures on reflectance and transmittance on variation of wavelength and at different angles of incidence
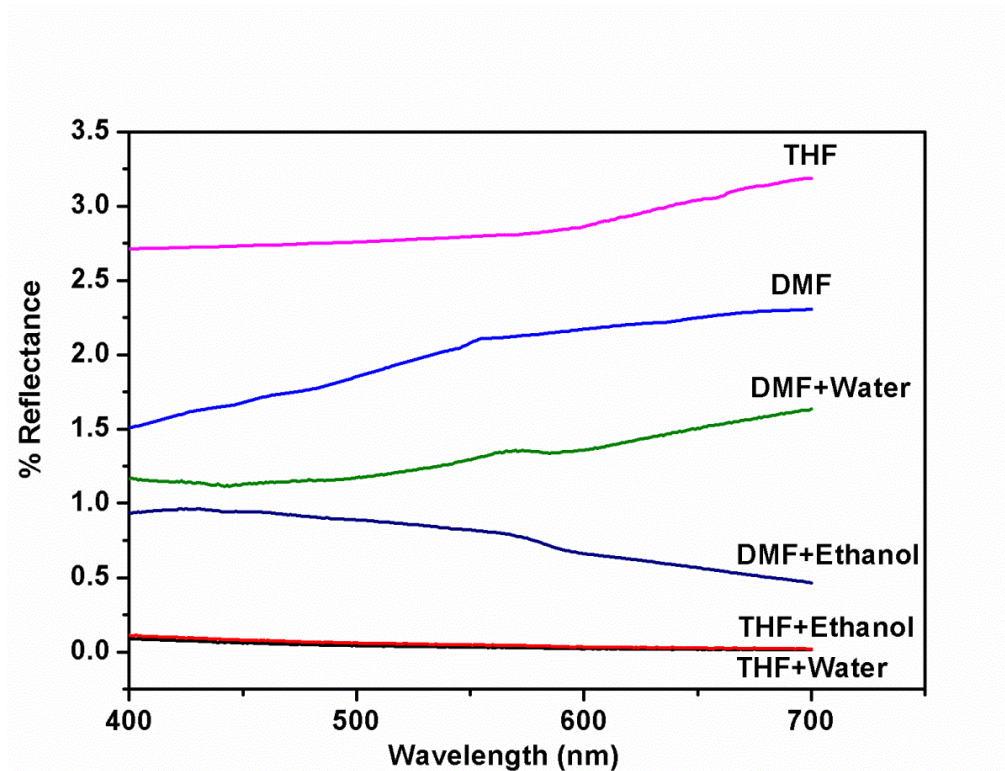
3.2.1 Reflectance with variation of wavelength

Fig. **13**: The reflectance of PS-b-PMMA porous films as a function of wavelength (300nm to 700nm) at 30 deg angle of incidence

Here we observe all the porous films are showing very low reflectance values in the entire visible region. Among all the six porous films samples, porous films of PS-b-PMMA (THF solvent) and DI water as non- solvent as well as PS-b-PMMA (THF solvent) and ethanol as non-solvent shows almost 0.1% reflectance. This is because of the surface phenomena where the entire light get trapped in between the porous structures and back reflected within the structures and finally mitigated. Thus no more reflected light from the surface of the film observed resulting in almost no reflectance. Coming to other samples, both the standard DMF (1.5-2%) and THF (2.75%) solvent based porous films shows high reflectance values compared to all. The reflectance values started steadily increasing with increase in wavelength. A steady increase is observed at starting 300 nm-400 nm in case of THF porous film
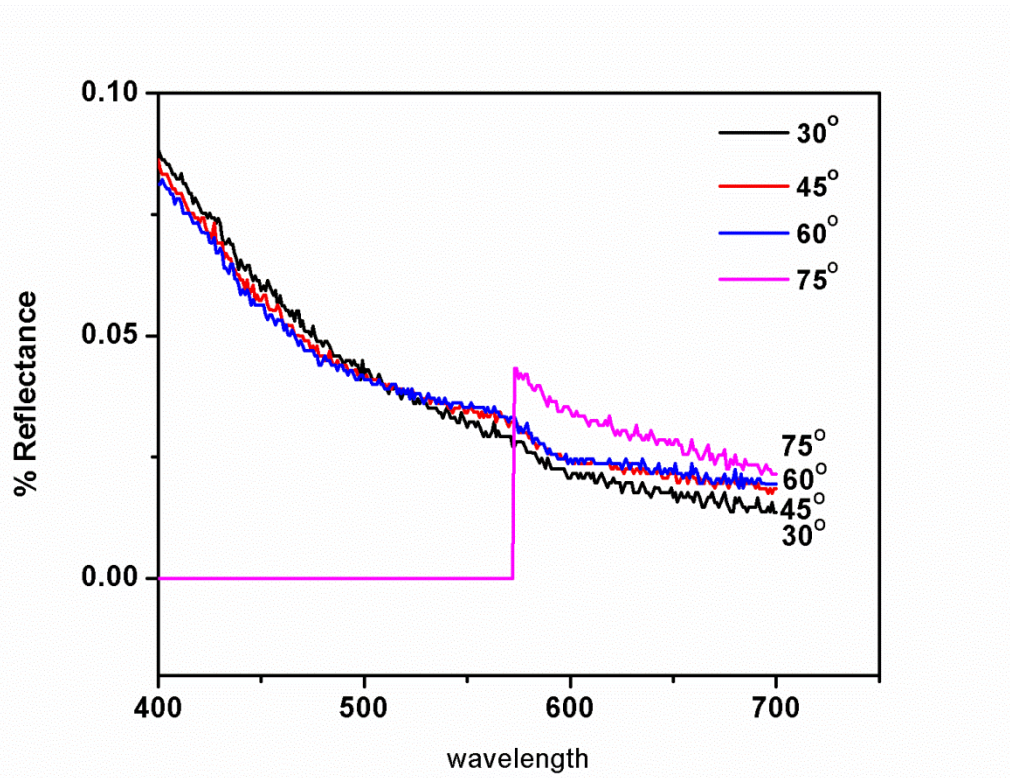
3.2.2 Reflectance with variable angle of incidence

Fig. **14**: Effect of incidence angle of light (30º, 45º, 60°& 75º) on reflectance properties for PS-b-PMMA Porous Film (THF-DI Water) samples

PS-b-PMMA Porous Film (THF-DI Water) samples were taken to observe the role of variable angle of incidence of light. Here in Fig. 14, at 75° angle of incidence very low reflectance phenomena i.e., 0.002% is observed till 570nm and suddenly increased to 0.04%. In all other cases, 30º, 45° &60º we found the values are almost merging and steadily decreasing with increase in wavelength. At these three angles we found reflectance values varied from 0.08% to 0.02% with increasing wavelength.
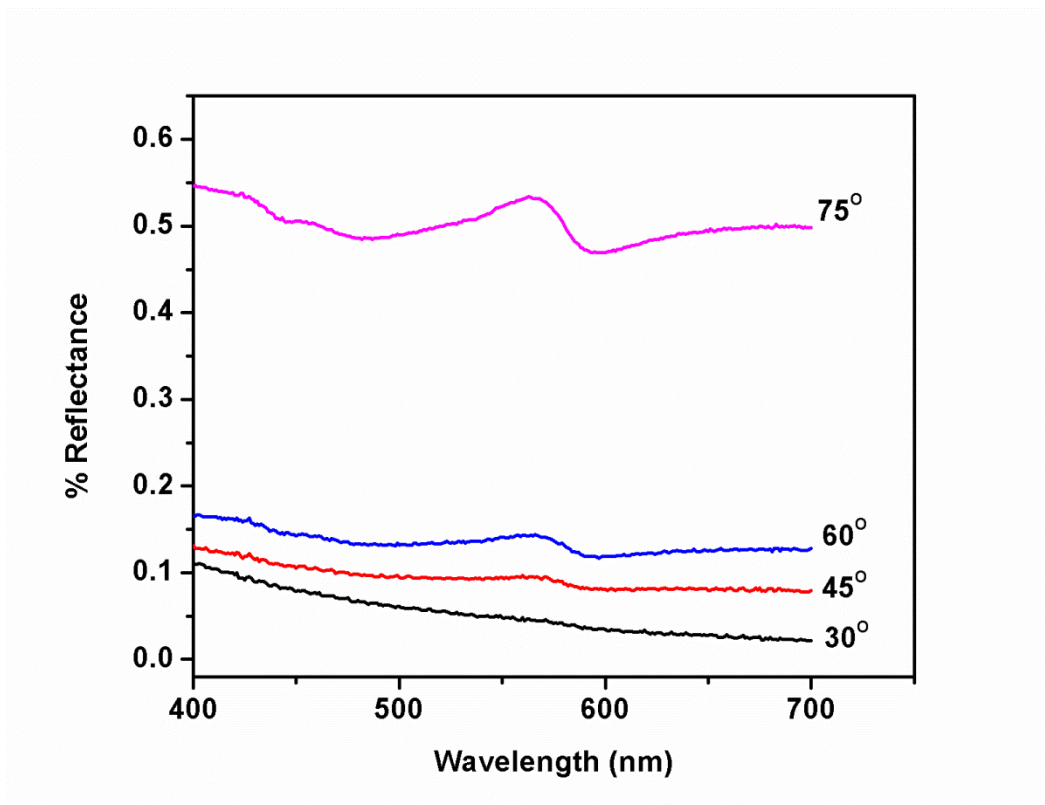
Fig **15**: Graph shows the effect of incidence angle (30º, 45º, 60º& 75º) of light on reflectance properties for PS-b-PMMA Porous Film (THF-ethanol) samples

In Figure 15, we observe that at 30º angle of incidence a low value of 0.11% reflectance is observed throughout the visible region and low value 0.45-0.55% observed at 75º incidence. On comparing with ethanol, as non-solvent THF-DI water porous samples showed good anti-reflective values at variable angle of incidence.
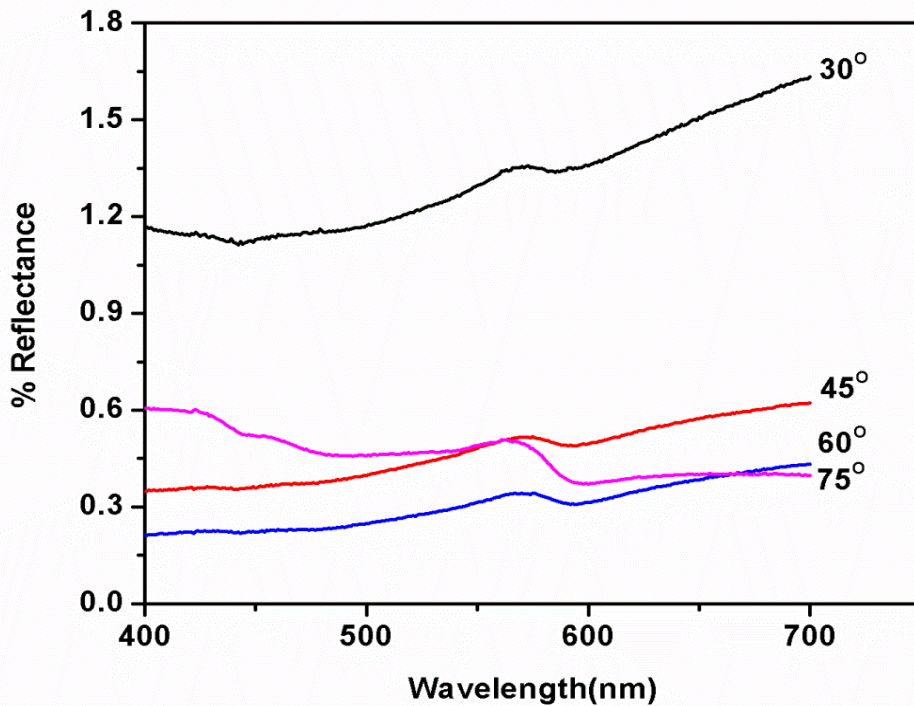
Fig 16: Graph shows the effect of incidence angle (30º, 45º, 60º& 75º) of light on reflectance properties for PS-b-PMMA Porous Film (DMF-DI water) samples

In the above Figure , at different angle of incidence, the porous films(DMF-DI) shows at 60º slight variation in the reflectance values showing steadily increase value in between 0.2%-0.3% and 1.1%-1.5% at 30º incidence.

The porous structures on the samples plays a vital role for obtaining these low reflectance values. Two samples of each porous film were prepared and the reflectance values were measured for better approximation in values.
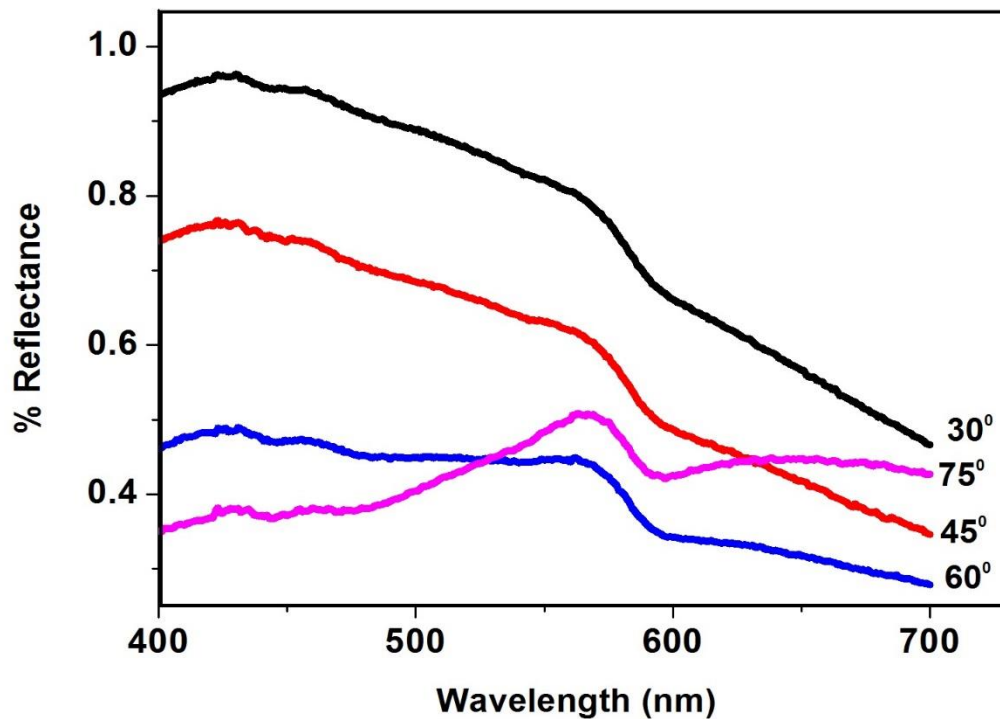
Fig **17**: Graph shows the effect of incidence angle (30º, 45º, 60º& 75º) of light on reflectance properties for PS-b-PMMA Porous Film (DMF-ethanol) samples

While in Figure 17, we observed that at all the angles, the reflectance values are steadily decreasing with increase in wavelength. As the angle of incidence increases at 600nm we observe a steep curve decrease in reflectance values. At 75º low reflectance of 0.3% observed and gradually increasing showing a stabilized value of 0.5% at 700nm.At 60º we found the reflectance% decreasing from 0.5% at 400nm to 0.1% at 700nm showing minimum notable value among all incident angles i.e. 30º, 45º and 75º

Finally from all the above results, we found in all cases minimum reflectance values are obtained at high angle of incidence (75º) except in the case of THF-ethanol samples. From all these

reflectance measurements we conclude these porous films with high surface roughness helps in minimizing the reflectance phenomena drastically to near-zero.

3.2.3 Transmittance studies

Transmittance is the fraction of incident light (electromagnetic radiation) at a specified wavelength that passes through a sample. Here we maintained the same instrument settings that were used for reflectance measurements.
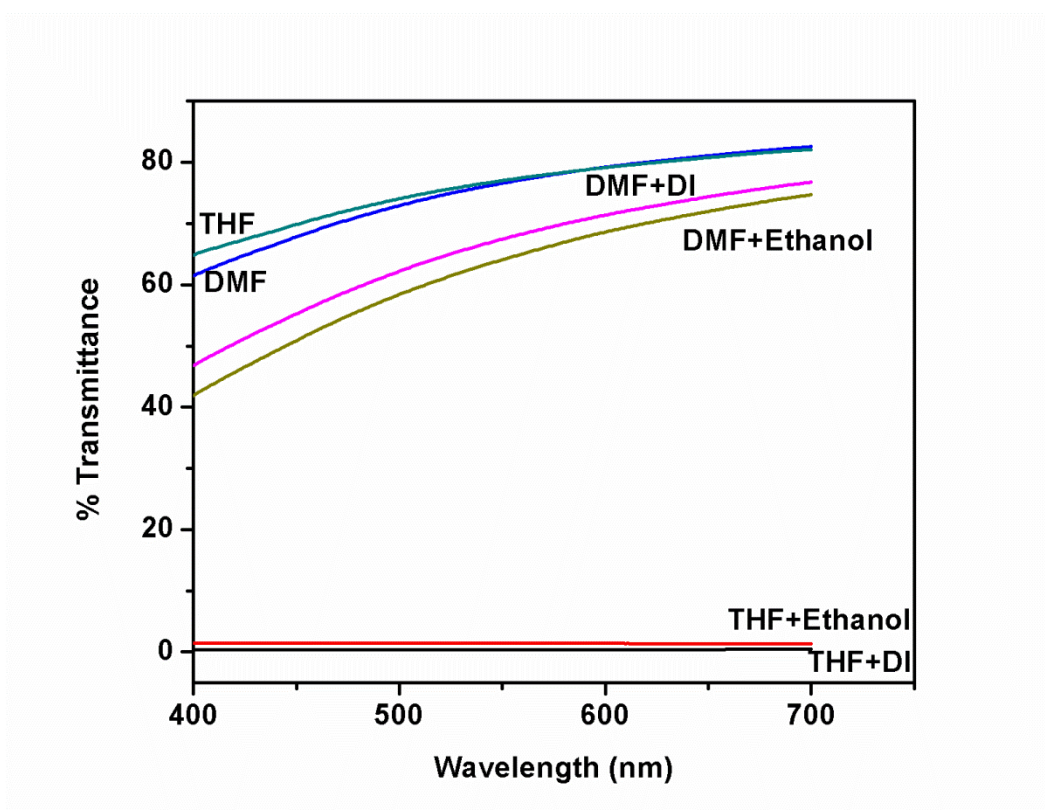

Fig **18**: Graph shows the transmittance of PS-b-PMMA porous films with variation of wavelength from 300nm to 700nm at 90 deg angle of incidence

The transmittance value of standard sample used in spectrophotometer shows 99% in entire visible region. Experiments were conducted at two different positions on the same sample for maintaining accuracy and approximation in obtained values. Here in Fig. 18, we observe the transmittance % for DMF-Ethanol and THF-Ethanol porous films almost zero throughout the region. Standard porous films shows a steadily increase of transmittance with increasing wavelength starting from 0% at 300nm and ending to 80% at 700 nm. DMF-ethanol and DMF-DI Water based porous films shows almost similar transmittance values of standard films (70-80%).

Low reflectance and low transmittance values thus signifies the high absorbance properties of the samples. Thus the absorbance properties of these samples clearly depict in the obtained results showing unsteady low values and slight and slow increase at higher wavelengths.

Chapter 4

Summary

In this work we studied role of surface roughness of polymer nanofibers and porous films on its optical properties. We used a simple and efficient method known as electrospinning for generation of beads and nanofibers. For fabrication of porous films, we used non-solvent induced phase separation process on thin films prepared using spin coater.

By preparing 8wt% & 16wt% molar concentrations of cellulose acetate polymer different structural morphologies i.e. beads and nanofibers were fabricated using silicon as a substrate. The change in surface morphology affects the surface roughness. This was analyzed by measuring roughness of the samples by using 3D optical profiler. The RMS value of fibers (8950 ± 150nm) is more compared to beads (5320 ± 120nm) observed. Effect of the surface roughness on optical properties like reflectance, transmittance were studied using spectrophotometer. Both the total and the specular reflectance/transmittance were measured in the visible spectral range by using UV-VIS spectrophotometer. The low reflectance (0.04%) & low transmittance (5%) measurements with high absorbance of cellulose acetate fibers shows a good sign of using the polymer nanofibers mat as for antireflective coating applications. In this work, we propose a low cost material to be used as an excellent absorber for solar collectors, to increase its thermal efficiency by high capacity to absorb solar radiation.

Furthermore we have demonstrated the fabrication of polymer surfaces with nanoscale roughness using DI water and ethanol as non-solvent and thus inducing phase separation. Using spin coating

repeatedly with non-solvent, asymmetric porous structures as characterized by SEM and AFM were found on these samples leading to the surface roughness. From 3-D AFM topography, it was observed that the surface roughness for PS-b-PMMA porous films (THF solvent) can be varied from ~55 nm to 320 nm. Reflectance/transmittance measurements as carried out using UV-Vis spectropmeter showed very low value of reflectance (0%-2%) and steady increase of transmittance values (0%-80%). Thus we conclude that using non -solvent induced phase separation technique a highly porous structure films over a large area can be easily fabricated with omnidirectional and broadband anti-reflective properties. The rough and porous polymer surfaces as fabricated in this work with near zero reflection over wide range of wavelength and incident angle of light may potentially be used for various engineering applications such as solar panels, optical displays, window screens, marine etc..

References:

[1] Ellmer, K; Klein, A: Rech, B; *Springer*, **2008,** 27-30

[2] Muller, J.; Schope, J.; Kluth, O.; Rech, B.; Sittinger, V.; Szyszka, B.; Geyer, Lechner. B; Schade, H;   Ruske, M ; Dittmar, G; Bochem H,P, ; *Thin Solid Films* **2003,**442*,* 158–162

[3]. Muller, J.; Kluth, O.; Wieder, S.; Siekmann, H.; Schöpe, G.; Reetz, W.; Vetterl, O.; Lundszien, D.; Lambertz, A.; Finger, F.; Rech, B.; Wagner, H; *Sol. Energy Mater. Sol. Cells* **2001** *66*, 275–281

[4]   Cai, H.; Zhang, D.; Xue, H; Tao, K; *Sol. Energy Mater. Sol. Cells* **2009**, 93, 1959–1962

[5]. Shetty P.K.; Theodore N.D.; Ren J.; Menendez, M.; Kim, H.C.; Misra, E.; Mayer, J.W.; Alford, T.L.; *Mater. Lett.* **2005**, 59, 872–875.

[6] Nelson, J.; the Physics of Solar Cells, London, **2003.**

[7] Heyde, M.; Rademann, K.; Capella, B.; Geuss, M.; Sturm, H.; Spangenberg, T.; Niehus, H.; *Rev. Sci. Instrum* **2001** ,72,136.

[8]. Murthy, J.K.; Grov, G.; S. Rudiger, S.; Unveren, E.; Kemnitz, E.; Fluorine J.;   *Sol-Gel Sci. Technol.* **2004,** 125, 937.

[9]. Palik, E.D.; Handbook of Optical Constants of Solids II, **1991.**

[10].Yamaguchi, N.; Tadanaga, T.; Matsuda, A.; Minami, T.; Tatsumisago, M.. *Sol-Gel Sci. Technol.* **2005**, *33(1),* 117

[11]. Nishii, J.; Kintaka, K.; Kawamoto, Y.; Mizutani, A.; Kikuta, K; *Ceram.Soc.* , **2003**, 112

[12]. H. Kikuta, H. Toyota, W. Yu, *Opt. Rev.* **2003,** *10 (2)*, 63.

[13] Kaless, A.; Schulz, U.; Munzert, P.; Kaiser, N.; *Surf. Coat. Technol.***2005**, *200 (1–4),* 58.

[14] Kaless, A.; Schulz U.; Munzert, P.; Kaiser, N.; *Surf. Coat. Technol.* **2005**, 200, 58.

[15] Fay, F.; Kroll, U.; Bucher, C.; Vallatsauvain, E.; Shah, A.; *Sol. Energy Mater. Sol. Cells* **2005,** 86, 385.

[16] Barankin M.D.; Gonzalez E.; Ladwig A.M.; Hicks, R.F.; *Sol. Energy Mater. Sol. Cells* 2007, 91, 24.

[17] Minami, T.; Ida, T. Miyata, S.; Minamino, Y.; *Thin Solid Films* **2003,**445, 268.

[18] Lou, X.B.; Shen, H.L.; Zhang, H.; Li, B.B.; *Trans. Nonferrous Met. Soc*. **2007**, 814.

[19] Penky, M.R.; Zartman, J., Krantz, W.B., Greenberg, A.R. and Todd, P.; *Journal of Membrane Science* **2003**, 211, 71-90.

[20] Altinkaya, A. S.; Ozbas, B.; *Journal of Membrane Science*, **2004**, 230, 71–89.

[21] Matsuyama, H.; Nishiguchi, M; and Kitamura, Y.; *Journal of Applied Polymer Science*, **2000,** 77, 776-782.

[22] Shojaie, S. S.; Krantz, W. B.; Greenberg, A. R.; *Journal of Membrane Science*, **1994,**94, 255 − 280.

[23] Shojaie, S. S.; Krantz, W. B.; Greenberg, A. R.; *Journal of Membrane Science*, **1994**, 94, 281 − 298

[24]Mulder, M.; Basic Principles of Membrane Film Technology, Kluwer Academic, Dordrecht, **1992**

[25] Van de Witte P.; Dijkstra P.J.; van den Berg, J.W.A.; Feijen, J.; *Journal of Membrane Science* 117, **1996** , 1-31.

[26] Dar-Jong Lin; Cheng-Liang Chang; Tzung-Chin Chen; Liao-Ping Cheng; *Desalination* **2002** 145,25–29